Electronic Supplementary Material (ESI) for Journal of Materials Chemistry A.
This journal is © The Royal Society of Chemistry 2022

Electronic Supplementary Information

Atomically dispersed Mn-N_4 electrocatalyst with high oxygen reduction reaction catalytic activity from metal organic framework ZIF-8 by minimal water assisted mechanochemical synthesis

Ziyan Kong,[a,b] Tao Liu,[a,b] Kun Hou*[a] and Lunhui Guan*[a]

a. CAS Key Laboratory of Design and Assembly of Functional Nanostructures, and Fujian Provincial Key Laboratory of Nanomaterials, Fujian Institute of Research on the Structure of Matter, Chinese Academy of Sciences, Fuzhou, Fujian 350002, P.R. China

b. College of Chemistry, Fuzhou University, Fuzhou 350108, Fujian, P.R. China.

* Corresponding Author: khou@fjirsm.ac.cn ; guanlh@fjirsm.ac.cn

Experimental

1.1 Chemicals

2-methylimidazole (2-mlm, 98%) and ZnO powder (99.99%) were obtained from Aladdin. Manganese chloride tetrahydrate ($MnCl_2 \cdot 4H2O$, 99%, Adamas-beta) was purchased from Admas-beta. Manganese acetate tetrahydrate ($Mn(OAc)_2 \cdot 4H_2O$, 99%), sodium acetate anhydrous (NaOAc, 99%); Iron chloride ($FeCl_3$, 97%); Zinc nitrate hexahydrate ($Zn(NO_3)_2 \cdot 6H_2O$, 99%); HCl (36.0-38.0%); H_2SO_4 (95.0-98.0%) were purchased from Sinopharm Chemical Co. Ltd. All reagents were used as received without further purification.

1.2 Preparation of ZIF-8 precursor by water assisted mechanochemical synthesis

In a typical synthesis, 2 g of 2-mlm, 0.5 g of ZnO powder (mole ratio 4:1) were mixed in a motar jar, different amounts of $Mn(OAc)_2 \cdot 4H_2O$ dissolved in 1 ml of water was added to obtain ZIF-8 precursors with a variety of manganese doping ratios. In detail, 0.1004, 0.1506 and 0.3012 g of $Mn(OAc)_2 \cdot 4H_2O$ was dissolved in 1 ml of water respectively and then added to the motar jar in each synthesis. The mixture was ball milled for 3 hours and centrifuged with methanol, the resultant metal organic framework ZIF-8 was labelled as ZIF-8-OAc-n (n=15, 10, 5 and refers to

ZnO/$Mn(OAc)_2 \cdot 4H_2O$ ratio). The ZIF-8 production yield (the ratio of actual product mass collected after centrifugation to theoretical product mass) was determined to be ~99.34%. For comparison, $MnCl_2 \cdot 4H_2O$ was used as an alternative manganese salt precursor instead of $Mn(OAc)_2 \cdot 4H_2O$ to prepare the ZIF-8 precursor, the obtained product was labelled as ZIF-8-Cl-n (n=15, 10, 5 and refers to ZnO/$MnCl_2$ ratios). The mechanochemical synthesis was conducted with planetary ball mill equipment (QM-3SP2, Nanjing NanDa Instrunment Plant)

1.3 Preparation of ZIF-8 precursor by solvothermal method

The synthesis was conducted follow a previous literature.[1] In detail, 2.63 g of 2-methylimidazole (32 mmol) was first dissolved in 30 ml methanol in a flask. Separately, 2.4 g of $Zn(NO_3)_2 \cdot 6H_2O$ (8 mmol) and 0.196 g of $Mn(OAc)_2 \cdot 4H_2O$ (0.8 mmol) were dissolved in 60 ml methanol in another flask. The $Zn(NO_3)_2 \cdot 6H_2O$ and $Mn(OAc)_2 \cdot 4H_2O$ methanol solution was added to the 2-methylimidazole solution under vigorous stirring. After stirred at room temperature for 1 hour, the while slurry was transferred to a Teflon-lined stainless-steel autoclave and kept at 120 °C for 4 h. The $Mn(OAc)_2 \cdot 4H_2O$ salt incorporated ZIF-8 was collected and washed with N,N-Dimethylformamide (DMF) for three times and methanol for two times, and finally dried at 70 °C under vacuum. 500 mg of $Mn(OAc)_2 \cdot 4H_2O$ incorporated ZIF-8 precursor was obtained and the yield was 44.74%.

1.3 Preparation of Mn-N-C and N-C catalysts

The ZIF-8 precursors synthesized by both mechanochemical grinding and solvothermal methods were first heated under N_2 atmosphere at 950 °C in a tube furnace for 1 hour. The carbon particles were termed Mn-N-C-OAc-n-First, Mn-N-C-Cl-n-First and Mn-N-C-Solvothermal-First (n=5, 10, 15, and it refers to the ZnO to manganese salt ratios. The Zn^{2+} to Mn^{2+} ratio was 10 in the solvothermal ZIF-8 derived sample). Then the samples were leached at 80 °C in 0.5 M H_2SO_4 solution for 5 h and dried under vacuum for 6h. The dried sample powder was dispersed into a solution ($V_{isopropanol}$: $V_{2\ M\ HCl}$ = 1:1) containing $MnCl_2$ and Urea. After ultrasonic treatment for 2 h and magnetic agitation for 7 h, the samples were collected through filtration and then dried in a vacuum oven at 80°C for 6 h. Finally, second pyrolysis was conducted at 950°C for 1 h in N_2 atmosphere to obtain the final Mn-N-C-OAc-n-Second catalysts, Mn-N-C-Cl-n-Second and Mn-N-C-Solvothermal-Second catalysts. The nitrogen doped carbon (N-C) was prepared by directly

pyrolyzing the ball milled ZIF-8 without manganese salt under N_2 at 950 ºC for 1 hour. Then the N-C sample was carried out the same experimental operation as Mn-N-C-OAc-n-Second, but no manganese salt was added during the process, and the final catalyst was termed N-C-Second.

1.4 Preparation of Fe-N-C catalysts

1 g of 2-mlm, 0.5 g of ZnO powder were mixed in a motar jar, $FeCl_3$ (0.0996 g) and NaOAc (0.1008 g) dissolved in 1 ml of water was added and followed by grinding for 3 hours, ZIF-8 doped with iron salt was obtained. The ZIF-8 precursor was heated at a temperature of 950 °C in a tube furnace under N_2 flow for 1 h to obtain the Fe-N-C-OAc-10-First catalysts. The sample was then treated with acid leaching in 0.5 M H_2SO_4 solution at 80 °C for 5 h. The dried sample powder was dispersed into a mixed solution ($V_{isopropanol}$: $V_{2\ M\ HCl}$ = 1:1) containing $FeCl_3$ and Urea. After ultrasonic treatment for 2 h and magnetic agitation for 7 h, the sample was collected through filtration and then dried in a vacuum oven at 80 °C for 6 h. Finally, another pyrolysis was conducted at 950 °C for 1 h in N_2 atmosphere to synthesize the final Fe-N-C-OAc-10-Second catalysts.

Characterization

The morphology structure of all the samples was investigated by field emission scanning electron microscopy (FE-SEM, SU8010). Transmission electron microscopy (TEM) and high-resolution TEM (HR-TEM) images were obtained by using the Tecnai F20 microscope. X-ray diffraction (XRD) characterization was performed on a Miniflex 600 diffractometer with Cu Kα X-rays (1.5406 Å). Raman spectroscopy was performed using a microscopic confocal Raman spectrometer (Labram HR800 Evolution) at 532 nm excitation. The surface chemical states of the samples were investigated through X-ray photoelectron spectroscopy (XPS, ESCALAB 250 Xi). N2 isothermal adsorption/desorption was recorded at 77K by Brunauer-Emmett-Teller (BET, Quantachrome Autoscorb-iQ2-XR). Samples were degassed at 120 °C for 6 h under vacuum before nitrogen physisorption measurements. The X-ray absorption fine structure spectra (Mn K-edge) were collected at BL11B station in Shanghai Synchrotron Radiation Facility (SSRF) .The Mn K-edge spectra of all the samples were recorded under fluorescence excitation mode using a

Lytle detector except for the Mn foil, which was measured with transmission mode. The XAS data were analyzed by the Athena and Artemis software.

Electrochemistry measurement

All electrochemical measurements were performed using a CHI electrochemical workstation (CHI760e) in a conventional three-electrode cell at room temperature. A rotating ring-disk electrode (RRDE) was used as the working electrode. Ag/AgCl (3.5 M KCl solution) and a graphite rod were used as reference and counter electrode, respectively. 0.1 M KOH solution and 0.1 M $HClO_4$ solution were applied as electrolyte, respectively. All potentials used in this work have been converted to the RHE scale. To prepare the catalyst ink, 5 mg catalyst powder was dispersed in 1 mL solution containing 960 μL isopropyl alcohol and 40 μL 5% Nafion solution by sonication for at least 1 h. Then a certain volume of the catalyst ink was pipetted onto the electrode surface with the nonprecious catalyst loading 0.8 mg cm^{-2} and the loading of Pt/C (20 wt% Pt) 0.3 mg cm^{-2}. Before ORR tests, N_2/O_2 flow was purged through the electrolyte in the cell for about 30 min and a flow of O_2 was maintained over the electrolyte during the measurements to ensure O_2 saturation. The cyclic voltammetry (CV) tests of the catalyst were measured in O_2-saturated 0.1 M KOH solution or 0.1M $HClO_4$ with a scan rate of 50 mV s^{-1}. The linear sweep voltammetry (LSV) of the catalyst was measured in O_2-saturated KOH (0.1 M) water solution with a rotation rate of 1600 rpm and O_2-saturated $HClO_4$ (0.1 M) water solution with a rotation rate of 900 rpm. The stability of the catalyst was studied by potential cycling from 0.6 to 1.0 V in 0.1 M KOH solution and 0.1 M $HClO_4$ solution at 25 °C, respectively.

The hydrogen peroxide yield (%H_2O_2) and the electron transfer number (n) of the catalysts were calculated using the following equations:

$$H_2O_2(\%)=\frac{200\times I_r}{N\times I_d+I_r}$$

$$n=\frac{4\times I_d}{I_d+\frac{I_r}{N}}$$

I_r and I_d are the ring and disk currents and N is the collection efficiency (0.36) of the disk

Zinc air battery fabrication

5 mg catalyst powder was dispersed in 1 mL solution containing 960 μL isopropyl alcohol and 40 μL 5% Nafion solution. Then, the slurry was sprayed on the hydrophobic carbon paper uniformly with the nonprecious catalyst loading 1 mg cm^{-2} and the loading of Pt/C (20 wt% Pt) 0.5 mg cm^{-2}.This carbon paper was used as the air cathode while a polished Zn foil was used as the anode. The two electrodes were assembled in a home-made zinc-air battery, while 6 M KOH aqueous solution was used as the electrolyte. The electrochemical measurement was then carried out on a CHI760e electrochemical station.

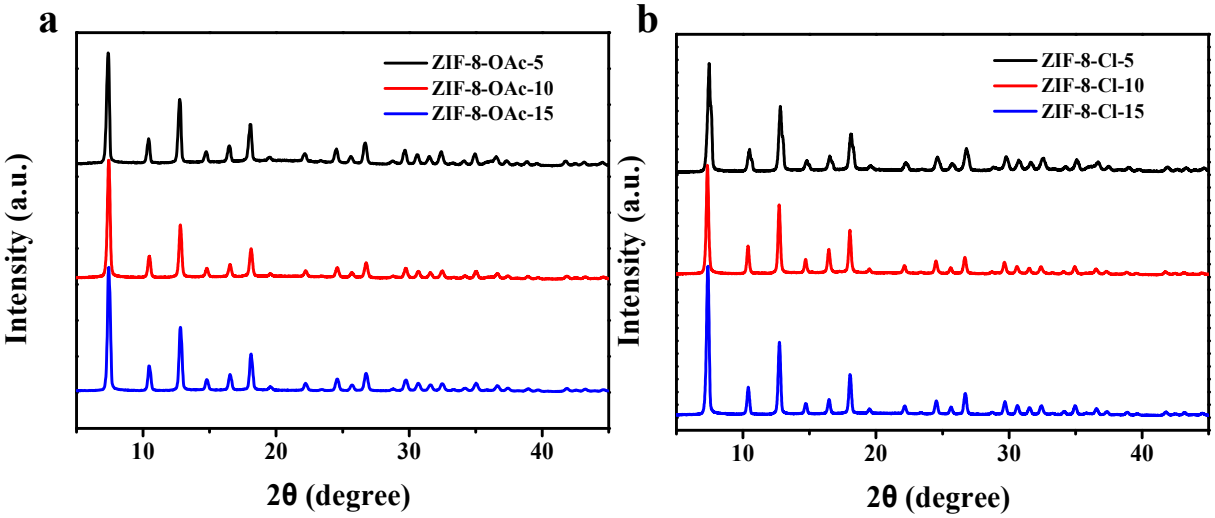

Figure S1. The X-ray diffraciton patterns of the (a) ZIF-8-OAc-n (n= 5, 10, 15) and (b) ZIF-8-Cl-n (n=5, 10, 15) from the mechano chemical synthesis.

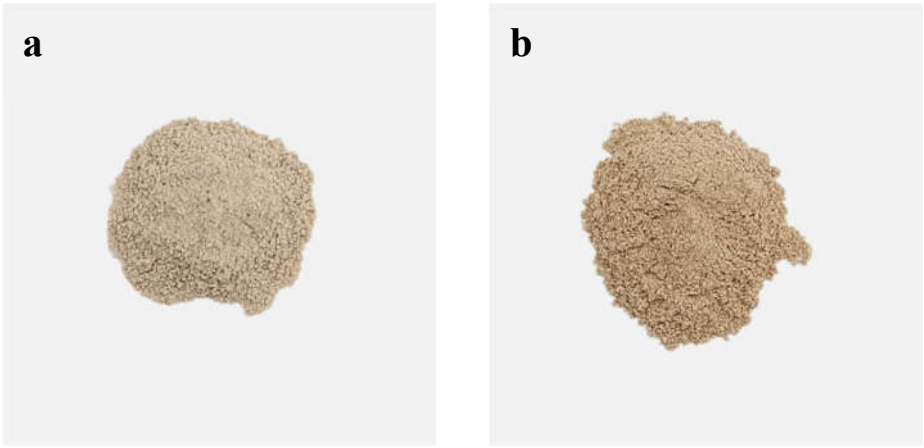

Figure S2 The picture of the mechanochemical synthesized ZIF-8 with (a) $Mn(OAc)_2 \cdot 4H_2O$ and (b) $MnCl_2 \cdot 4H_2O$.

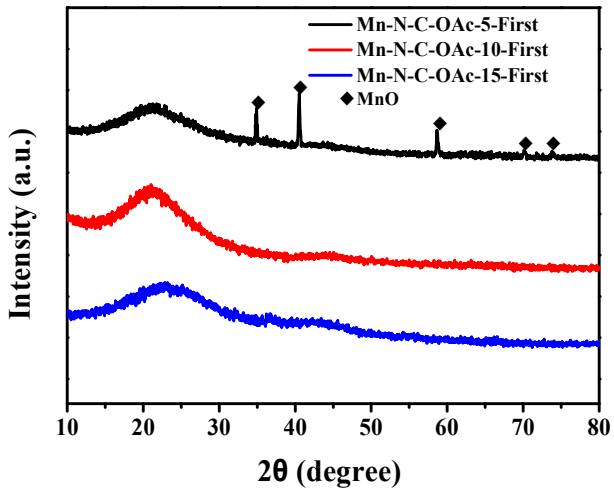

Figure S3 The X-ray diffraction patterns of the Mn-N-C-OAC-n-First (n=15, 10, 5) carbon particles after first thermal activation. MnO phase was detected when the ZnO to $Mn(OAc)_2$ ratio was 5.

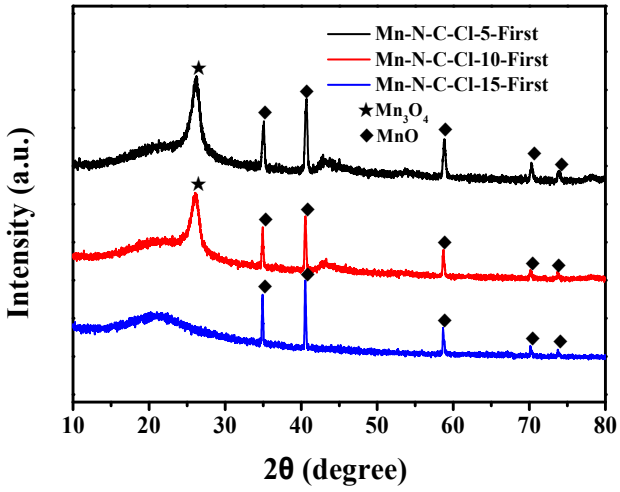

Figure S4 The X-ray diffraction patterns of the Mn-N-C-Cl-n-First (n=15, 10 and 5) carbon particles after first thermal activation. MnO phase was detected when the ZnO to $Mn(OAc)_2$ ratio was 15. All the samples were acid leached before XRD measurements.

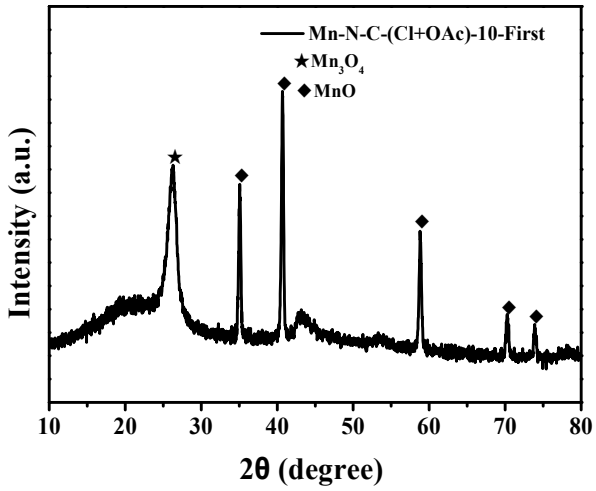

Figure S5 The X-ray diffraction (XRD) pattern of the Mn-N-C-(Cl+OAc)-10-First carbon particles after first thermal activation. The synthesis of the ZIF-8 precurosr was the same as that for Mn-N-C-Cl-10-First, except that NaOAc (0.1011 g, 1.24 mmol) was dissolved in the $MnCl_2 \cdot 4H_2O$ solution and added into the motar jar. The Mn-N-C carbon particle was termed as Mn-N-C-(Cl+OAc)-10-First.

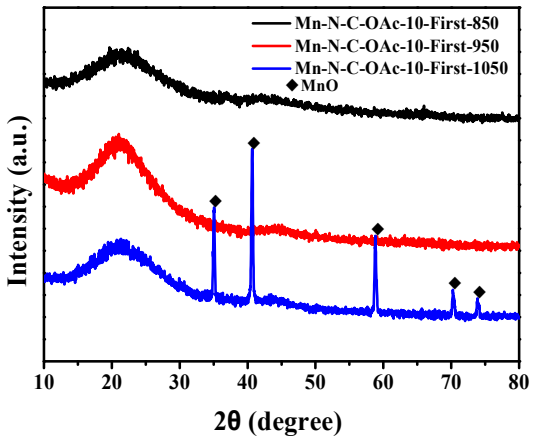

Figure S6 The X-ray diffraction patterns of the Mn-N-C-OAc-10-First-T (T=850, 950, 1050 °C) carbon particles after first thermal activation. MnO phase was detected when the pyrolysis temperature was 1050 °C.

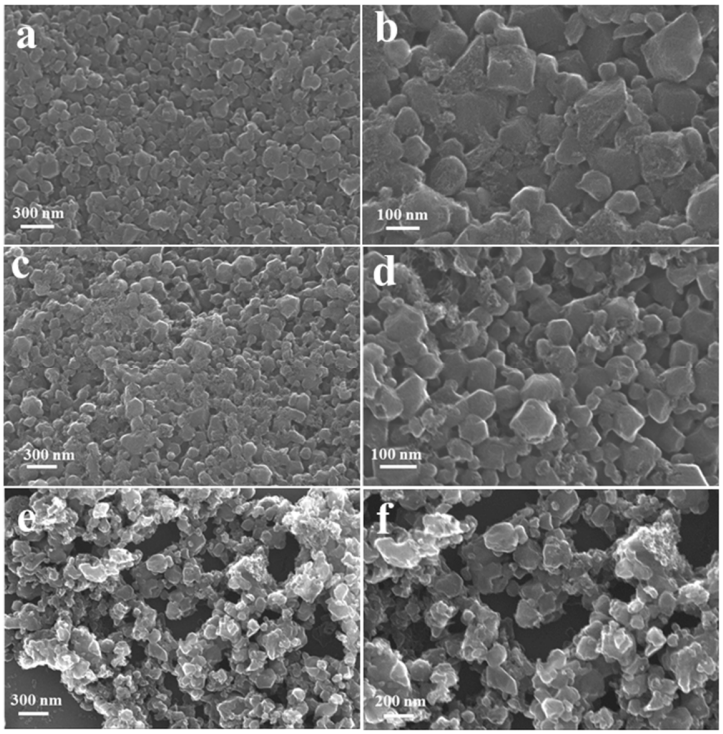

Figure S7 SEM images of Mn-N-C materials after first thermal treatment from ZIF-8 precursors with different $Mn(OAc)_2$ to ZnO ratios, (a&b) 1:15, (c&d) 1:10, (e &f) 1:5.

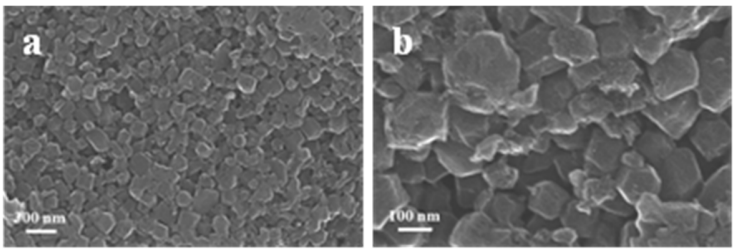

Figure S8 SEM images of Mn-N-C-OAc-10-Second.

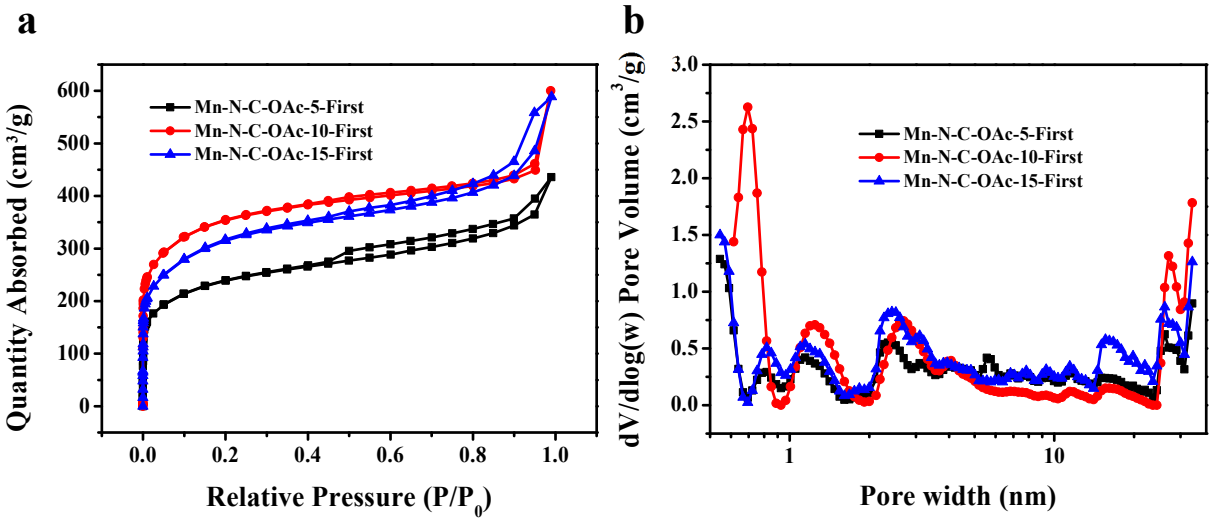

	BET surface area (m^2/g)	Micropore area (m^2/g)
Mn-N-C-OAc-5-First	856	579
Mn-N-C-OAc-10-First	1278	970
Mn-N-C-OAc-15-First	1147	813

Figure S9 (a) The N_2 adsorption-desorption curves of the Mn-N-C catalyst using $Mn(OAc)_2 \cdot 4H_2O$ as the manganese salt precursor; (b) The corresponding pore size distribution of the Mn-N-C catalysts with different initial $Mn(OAc)_2 \cdot 4H_2O$ doping ratios. The surface area and micropore surface was displayed in the table below the figure.

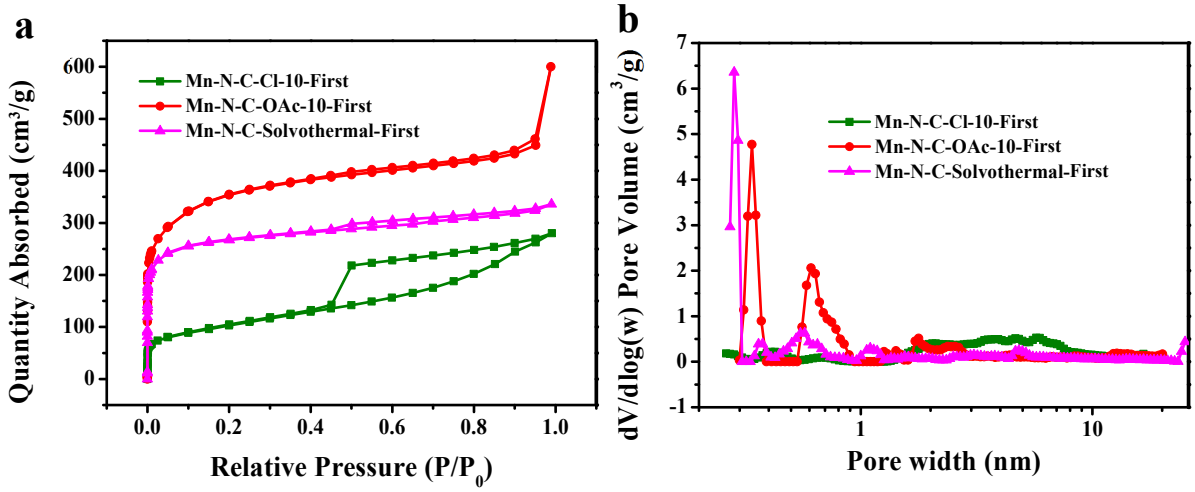

	BET surface area (m^2/g)	Micropore area (m^2/g)
Mn-N-C-Cl-10-First	362	80
Mn-N-C-OAc-10-First	1278	970

Mn-N-C-Solvothermal-First	1010	853

Figure S10 (a) The N_2 adsorption-desorption curves of Mn-N-C-Cl-10-First, Mn-N-C-OAc-10-First , Mn-N-C-Solvothermal-First catalyst; (b) The corresponding pore size distribution of Mn-N-C-Cl-10-First, Mn-N-C-OAc-10-First , Mn-N-C-Solvothermal-First catalyst. The surface area and micropore surface was displayed in the table below the figure.

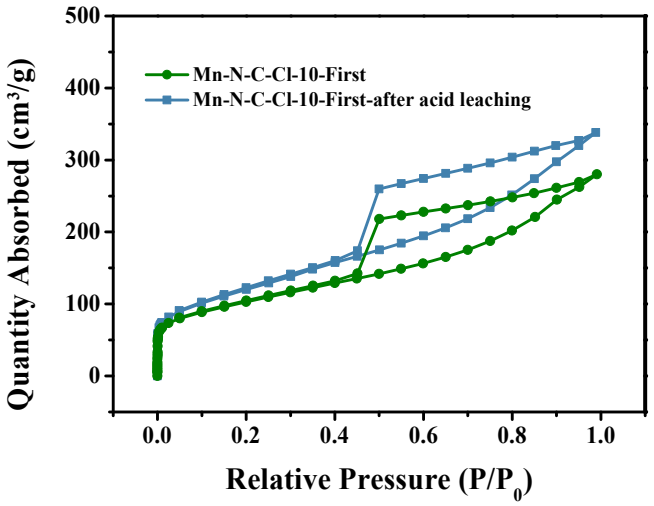

	BET surface area (m^2/g)	Micropore area (m^2/g)
Mn-N-C-Cl-10-First	362	80
Mn-N-C-Cl-10-First-after acid leaching	427	69

Figure S11 The N_2 adsorption-desorption curves of the Mn-N-C carbon particles after first thermal pyrolysis using $MnCl_2 \cdot 4H_2O$ incorporated ZIF-8 as the precursor. The Mn-N-C carbon particles were treated with or without acid to show the impact of acid leaching on the carbon particle surface area, as well its effect to remove manganese oxides. The surface area and micropore surface was displayed in the table below the figure.

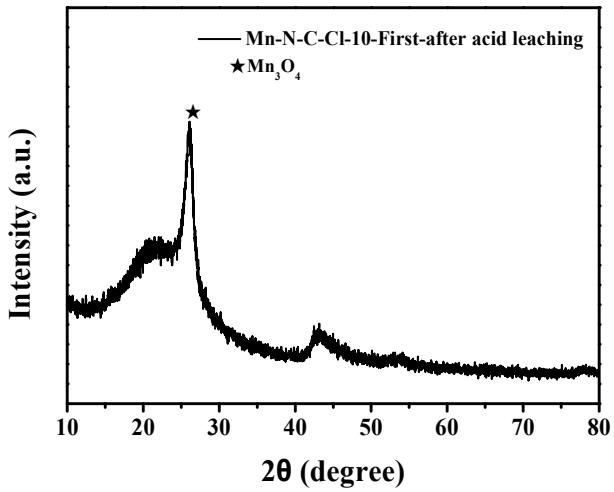

Figure S12 The X-ray diffraction patterns of the Mn-N-C-Cl-10-First carbon particles after acid leaching.

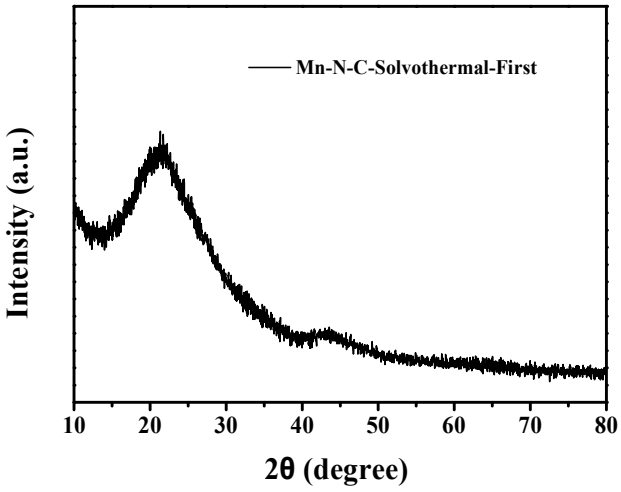

Figure S13 The X-ray diffraction patterns of the Mn-N-C-Solvothermal-First sample.

Table S1. The Full widths at half maximum (FWHM) and the I_D/I_G value of Mn-N-C catalysts.

Samples	FWHM (cm^{-1})		I_D/I_G
	D	G	
Mn-N-C-Cl-10-Second	84.53	71.82	1.05
Mn-N-C-OAc-10-Second	187.29	90.88	1.10
Mn-N-C-Solvothermal-Second	152.84	90.40	1.09

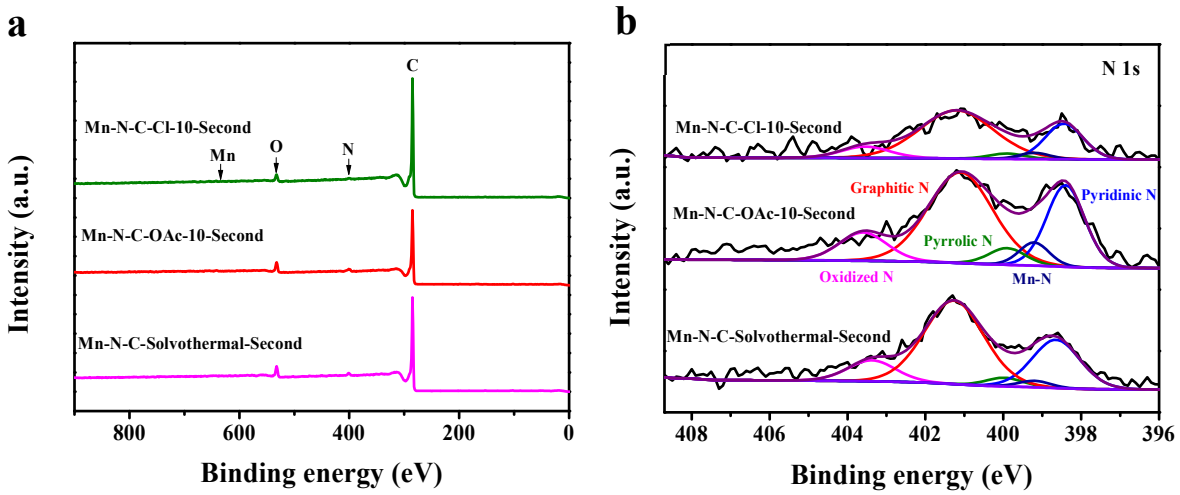

Figure S14 (a) XPS survey spectra of Mn-N-C-Cl-Second, Mn-N-C-OAc-Second and Mn-N-C-Solvothermal-Second catalysts; (b) N 1s high-resolution XPS spectra of Mn-N-C-Cl-Second and Mn-N-C-OAc-Second Mn-N-C-Solvothermal-Second catalysts.

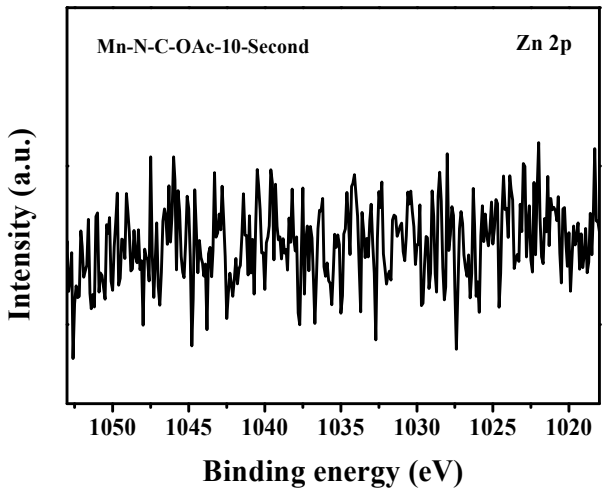

Figure S15 Zn 2p high-resolution XPS spectra of Mn-N-C-OAc-10-Second catalyst.

Table S2. The elements composition of the three Mn-N-C catalysts determined by XPS.

Samples	C (at.%)	N (at.%)	O (at.%)	Mn (at.%)
Mn-N-C-Cl-10-Second	94.81	1.46	3.52	0.21
Mn-N-C-OAc-10-Second	89.02	3.51	7.11	0.36
Mn-N-C-Solvothermal-Second	91.78	2.45	5.56	0.22
Mn-N-C-OAc-10-First	85.27	8.51	5.93	0.29
N-C-Second	91.56	3.71	4.73	/

Table S3. The category of the N species in the three catalysts. The N1s peaks were deconvoluted into five peaks and the atomic ratio of each nitrogen species was determined.

Content (at. %)	Pyridinic N (398.3 eV)	Mn-N (399.2 eV)	Pyrrolic N (399.9 eV)	Graphitic N (401.1 eV)	Oxidized N (403.6 eV)
Mn-N-C-Cl-10-Second	23.22	3.25	3.52	60.77	9.5
Mn-N-C-OAc-10-Second	26.66	5.96	5.31	50.43	11.64
Mn-N-C-Solvothermal-Second	26.39	1.82	2.52	59.11	10.16

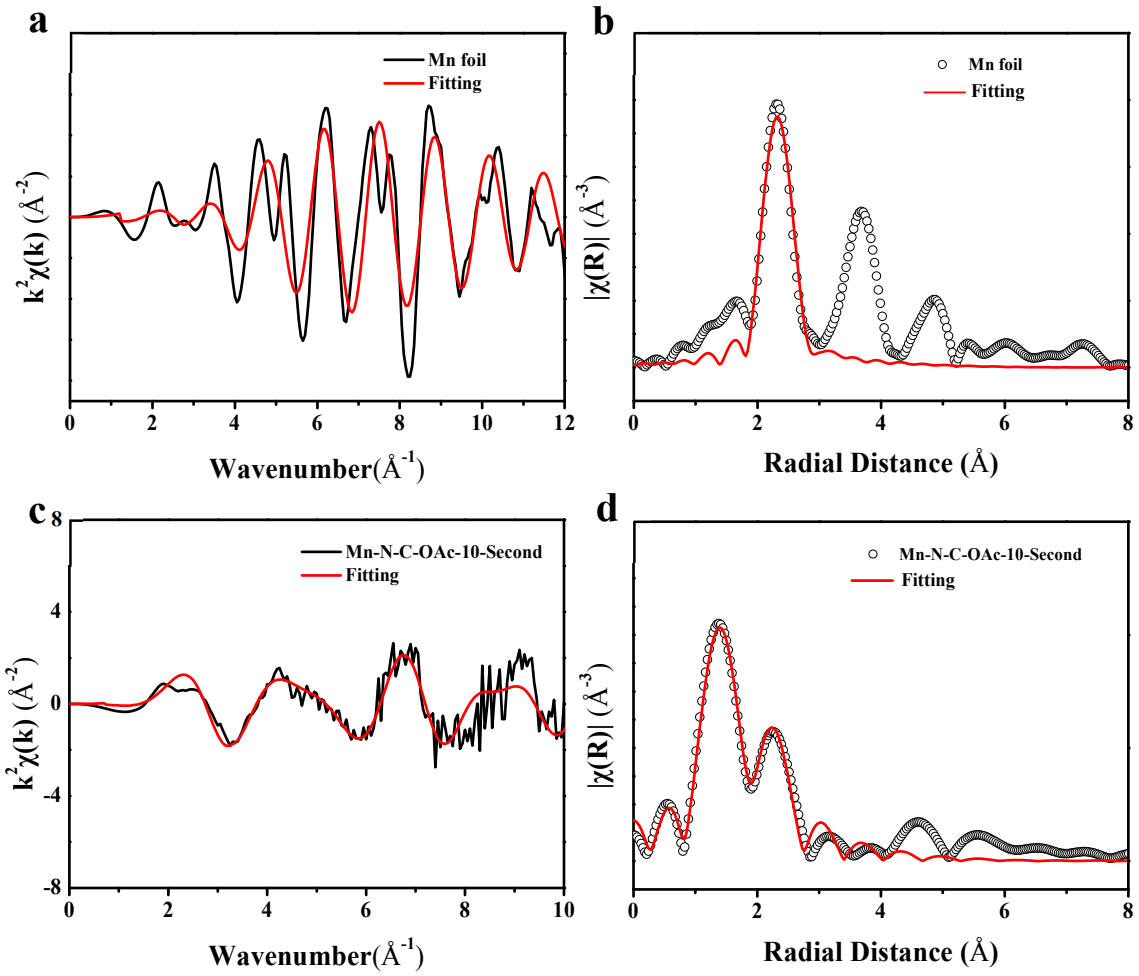

Figure S16 The k space and FT-EXAFS fitting curves of (a &b) Mn foil and (c &d) Mn-N-C-OAc-10-Second at Mn K-edge. The amplitude reduction factor (S_0^2) was extracted from the fitting of the Mn foil. The coordination numbers of Mn foil were fixed as the nominal values in the fitting. The obtained S_0^2 (0.85) was used for the subsequent fitting of Mn K-edge.

Table S4. EXAFS fitting parameters at the Mn K-edge various samples（S_0^2=0.85）

Sample	Path	CN	R (Å)	$\sigma^2\times10^3$ (Å^2)	ΔE (eV)	R factor
Mn foil	Mn-Mn	12*	2.67±0.01	6.1±1.9	5.9±2.5	0.016
Mn-N-C-OAc-10-Second	Mn-N	3.8±1.4	1.94±0.02	3.7±3.6	2.0±3.8	0.017
	Mn-C	5.8±2.5	2.84±0.03			

[a]*CN*: coordination number; [b]*R*: bond distance; [c]σ^2: Debye-Waller factors; [d] Δ*E*: the inner potential correction. *R* factor: goodness of fit. * the experimental EXAFS fit of metal foil by fixing CN as

the known crystallographic value.

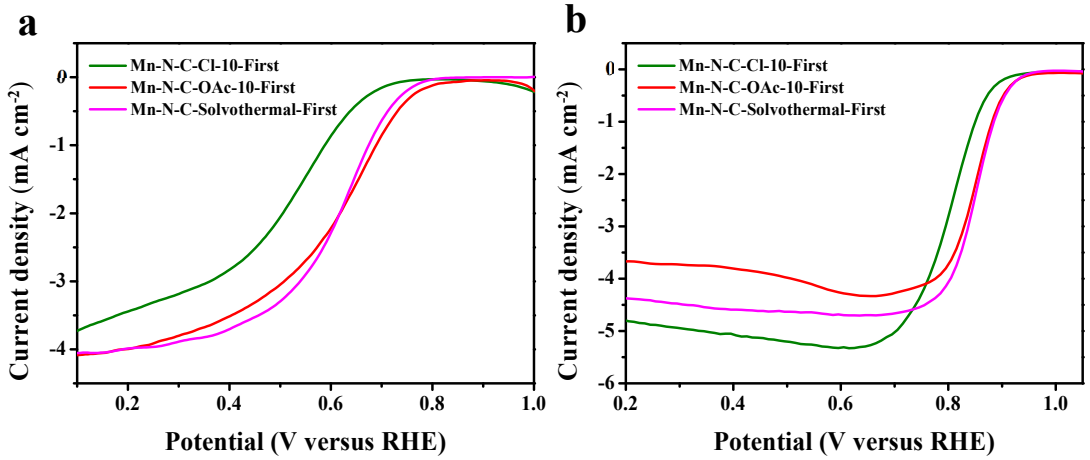

Figure S17 LSV curves of the Mn-N-C-Cl-10-First, Mn-N-C-OAc-10-First and Mn-N-C-Solvothermal-First in (a) 0.1 M $HClO_4$ solution and in (b) 0.1 M KOH solution.

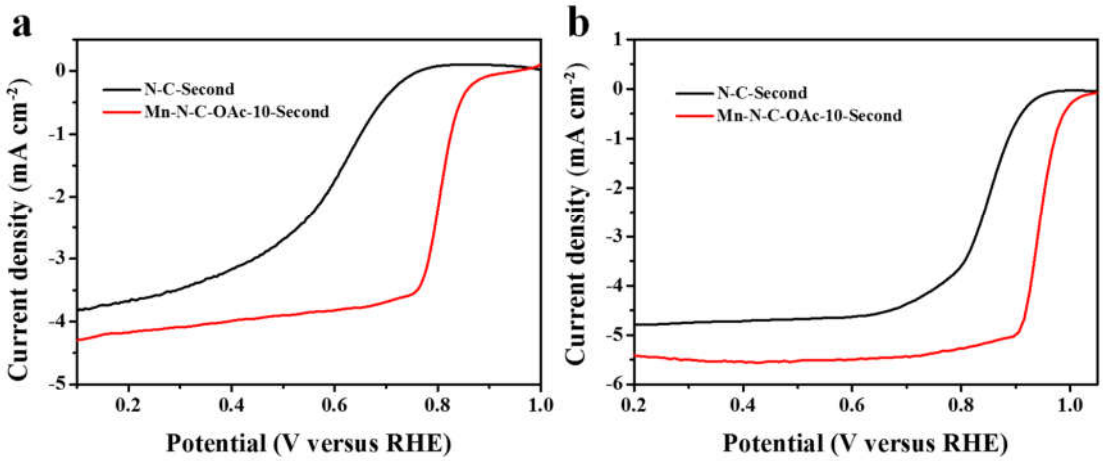

Figure S18 LSV curves of the N-C-Second (the same preparation method as Mn-N-C-OAc-10-Second, and without manganese salt) and Mn-N-C-OAc-10-Second catalysts in (a) 0.1 M $HClO_4$ solution and in (b) 0.1 M KOH solution.

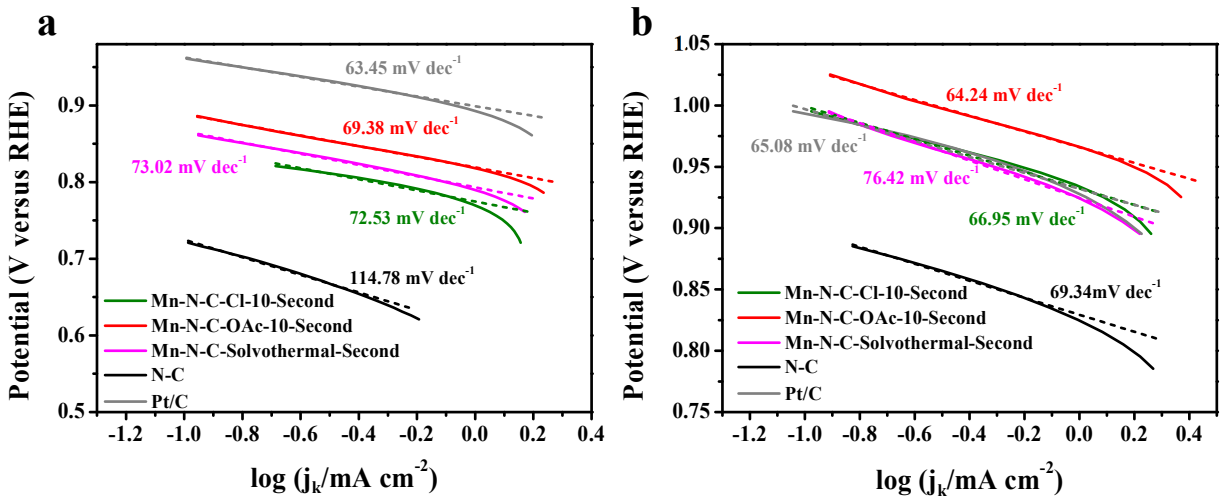

Figure S19 The Tafel plots of Mn-N-C catalysts and Pt/C in (a) 0.1 M $HClO_4$ and (b) 0.1 M KOH solution.

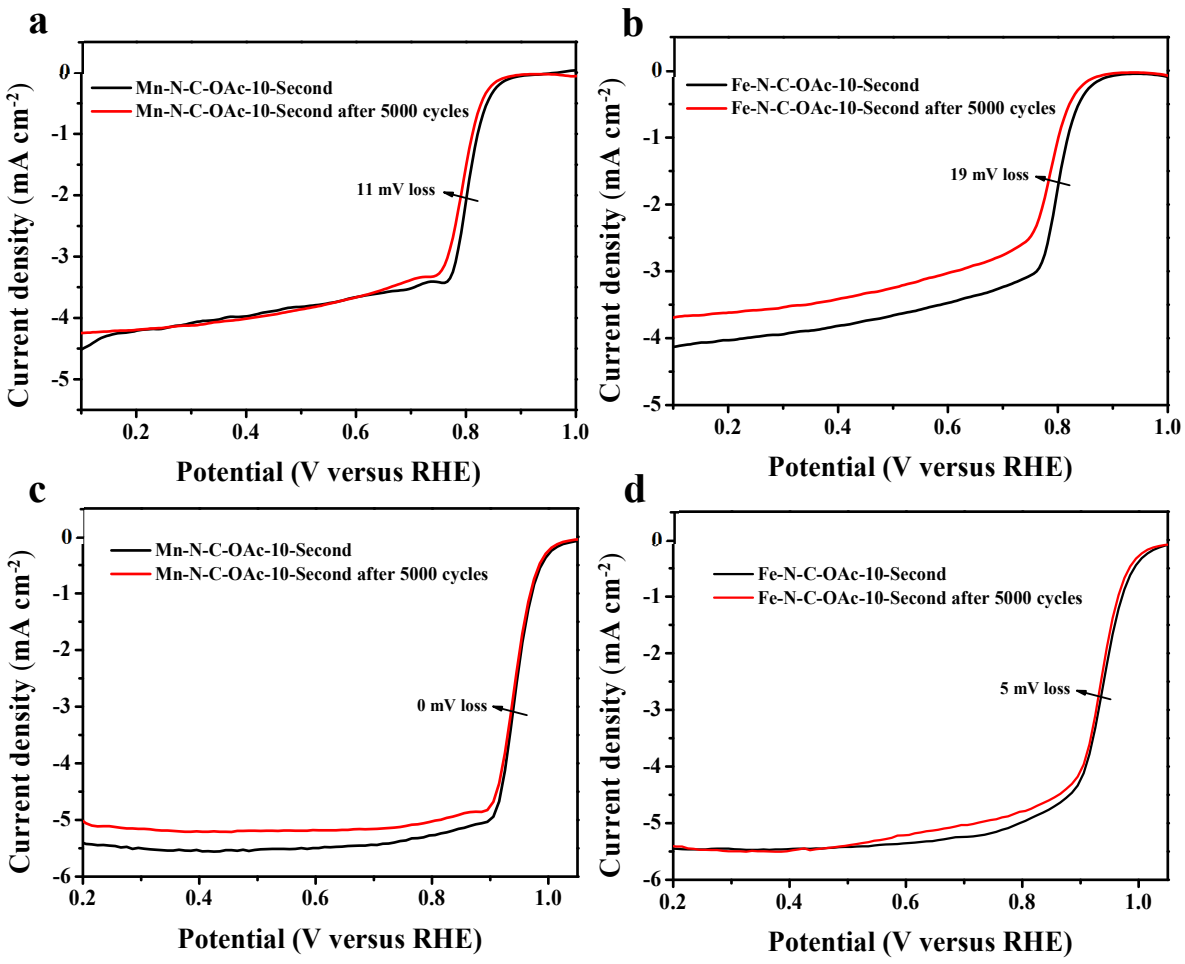

Figure S20 The stability study of the Mn-N-C catalyst. The catalysts were cycled from 0.6 V to 1.0 V for 5000 cycles before LSV study. Steady state LSV plots (a) Mn-N-C and (b) Fe-N-C in 0.1 M $HClO_4$ solution; (c) Mn-N-C and (d) Fe-N-C in 0.1 M KOH solution.

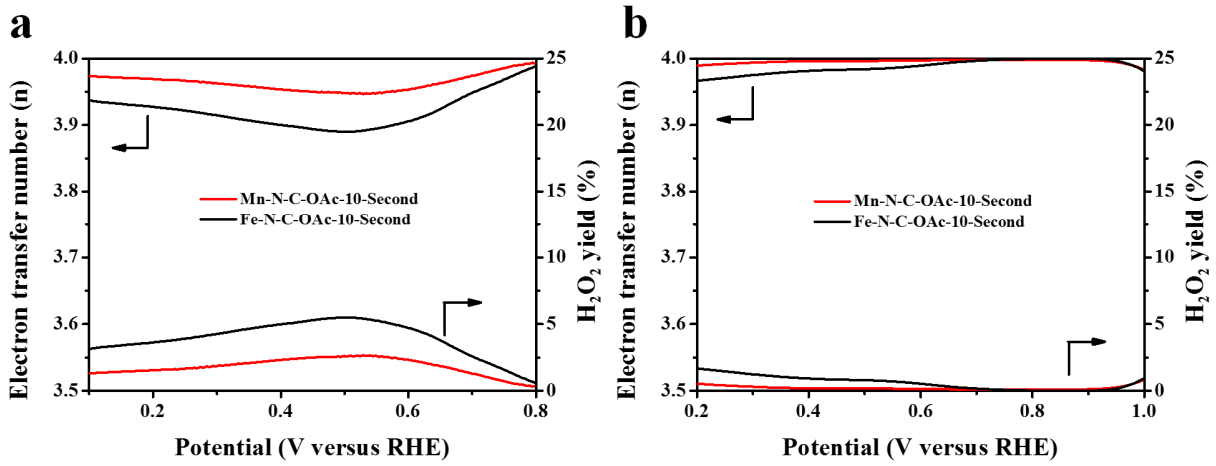

Figure S21. The electron transfer number and the H_2O_2 yield of Mn-N-C-OAc-10-Second and Fe-N-C-OAc-10-Second catalysts in (a) 0.1 M $HClO_4$ solution and (b) 0.1 M KOH solution.

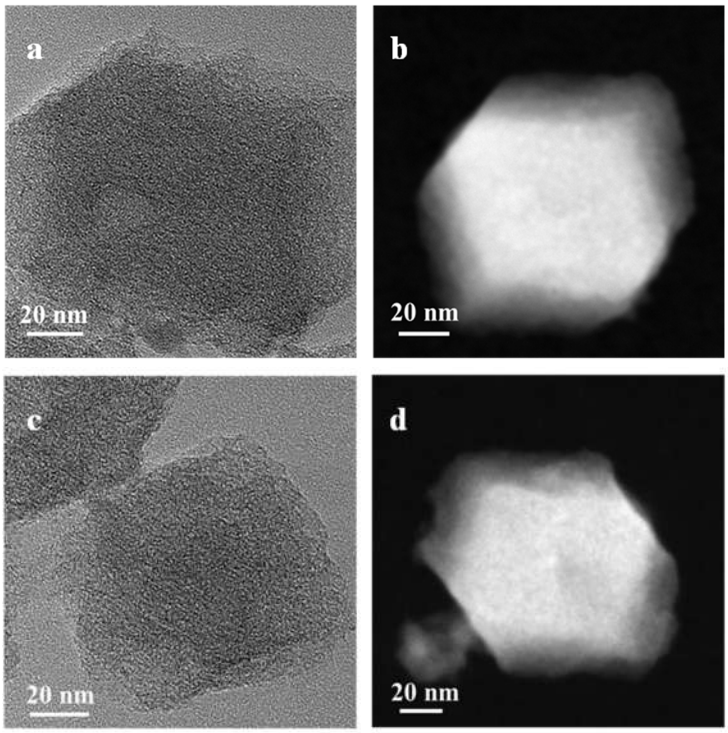

Figure S22. The high-resolution TEM and STEM of Mn-N-C-OAc-10-Second catalyst after 5000 potential cycles in 0.1 M $HClO_4$ (a, b) solution and 0.1 M KOH (c, d) solution.

Table S5. Summary of previously reported Mn-based carbon catalysts in terms of their ORR performances.

Catalysts	$E_{1/2}$/V (vs.RHE)		Reference
	acid	base	
Mn-SAS/CN	--	0.910 (1600 rpm)	[1]
g-SA-Mn-900	--	0.900 (1600 rpm)	[2]
MnNC-PDA-700	--	0.870 (1600 rpm)	[3]
Mn-N-C	0.780 (900 rpm)	--	[4]
Mn-NAHPC-900	0.730 (1600 rpm)	0.860 (1600 rpm)	[5]
Mn-N_2C_2	0.710 (1600 rpm)	0.915 (1600 rpm)	[6]
Mn-N_4-C_xS_y	--	0.916 (1600 rpm)	[7]
20Mn-NC-second	0.800 (900 rpm)	--	[8]
Mn-N-C-OAc-10-Second	0.803 (900 rpm)	0.944 (1600rpm)	This work

Table S6. Comparison of zinc-air battery performance between Mn-N-C-OAc-10-Second based zinc-air battery and other Mn-based zinc-air batteries in literature.

Catalyst	Catalyst Loading (mg cm^{-2})	Maximal Power Density (mW cm^{-2})	Reference
g-SA-Mn-900	2.0	147	[2]
MnNC-PDA-700	2.0	122.7	[3]
Mn-N-C900	1.0	132	[9]
MCG-2	2.0	112.38	[10]
Mn-N-C-OAc-10-Second	1.0	183	This work

References

1 X. Han, T. Y. Zhang, W. X. Chen, B. Dong, G. Meng, L. R. Zheng, C. Yang, X. M. Sun, Z. B. Zhuang, D. S. Wang, A. J. Han and J. F. Liu, *Advanced Energy Materials*, 2021, 11, 9.

2 Q. Y. Zhou, J. J. Cai, Z. Zhang, R. Gao, B. Chen, G. B. Wen, L. Zhao, Y. P. Deng, H. Z. Dou, X. F. Gong, Y. L. Zhang, Y. F. Hu, A. P. Yu, X. L. Sui, Z. B. Wang and Z. W. Chen, *Small Methods*, 2021, 5, 9.

3 H. Tian, X. Z. Cui, H. L. Dong, G. Meng, F. T. Kong, Y. F. Chen, L. X. Peng, C. Chen, Z. W. Chang and J. L. Shi, *Energy Storage Materials*, 2021, 37, 274-282.

4 K. X. Liu, Z. Qiao, S. Hwang, Z. Y. Liu, H. G. Zhang, D. Su, H. Xu, G. Wu and G. F. Wang, *Applied Catalysis B-Environmental*, 2019, 243, 195-203.

5 P. F. Tian, J. B. Zang, L. Dong, S. W. Song, S. Y. Zhou, H. W. Gao, X. Q. Tian and Y. H. Wang, *International Journal Of Hydrogen Energy*, 2021, 46, 543-554.

6 H. S. Shang, W. M. Sun, R. Sui, J. J. Pei, L. R. Zheng, J. C. Dong, Z. L. Jiang, D. N. Zhou, Z. B. Zhuang, W. X. Chen, J. T. Zhang, D. S. Wang and Y. D. Li, *Nano Lett.*, 2020, 20, 5443-5450.

7 H. S. Shang, Z. L. Jiang, D. N. Zhou, J. J. Pei, Y. Wang, J. C. Dong, X. S. Zheng, J. T. Zhang and W. X. Chen, *Chem. Sci.*, 2020, 11, 5994-5999.

8 J. Li, M. Chen, D. A. Cullen, S. Hwang, M. Wang, B. Li, K. Liu, S. Karakalos, M. Lucero, H. Zhang, C. Lei, H. Xu, G. E. Sterbinsky, Z. Feng, D. Su, K. L. More, G. Wang, Z. Wang and G. Wu, *Nature Catalysis*, 2018, 1, 935-945.

9 Y. Q. Wang, X. R. Zhang, S. B. Xi, X. Xiang, Y. H. Du, P. S. Chen, D. D. Lyu, S. B. Wang, Z. Q. Tian and P. K. Shen, *ACS Sustainable Chemistry & Engineering*, 2020, 8, 9367-9376.

10 Y. H. Pang, Z. Y. Mo, H. Wang, X. Y. Wang, V. Linkov and R. F. Wang, *ACS Sustainable Chemistry & Engineering*, 2021, 9, 5526-5535.